Eur. Phys. J. A (2013) **49**: 9
DOI 10.1140/epja/i2013-13009-8

THE EUROPEAN PHYSICAL JOURNAL A

Special Article – Tools for Experiment and Theory

An endoscopic detector for ultracold neutrons

L. Göltl[1,2], Z. Chowdhuri[1], M. Fertl[1,2], F. Gray[3], R. Henneck[1], K. Kirch[1,2], B. Lauss[1,a], T. Lefort[4], A. Mtchedlishvili[1], P. Schmidt-Wellenburg[1], and G. Zsigmond[1]

[1] Laboratory for Particle Physics, Paul Scherrer Institute, CH-5232 Villigen-PSI, Switzerland
[2] Institute for Particle Physics, ETH Zürich, Zürich, Switzerland
[3] Regis University, Denver, CO 80221, USA
[4] Laboratoire de Physique Corpusculaire, Université de Caen, CNRS/IN2P3, France

Received: 14 May 2012 / Revised: 18 October 2012
Published online: 21 January 2013 –
Communicated by B.R. Fulton

Abstract. A new versatile detector for ultracold neutrons (UCN) has been built and operated which combines multi-pixel photon counters and GS10 lithium-doped scintillators. Such detectors can be very small and can be used to monitor UCN inside storage vessels or guides with negligible influence (of order 10^{-6}) on the UCN intensity itself. We have shown that such detectors can be used in a very harsh radiation environment of up to 200 Gy/h via the addition of a 4 m long quartz light guide in order to place the radiation-sensitive photon counters outside the hot zone. Additionally we have measured the UCN storage times *in situ* in this harsh environment.

1 Introduction

We report on the development of a very small, versatile ultracold neutron (UCN) detector system, the adaptation of this detector to a harsh radiation environment, and its installation inside the accelerator-based UCN source at the Paul Scherrer Institute (PSI) in Switzerland. The basic detector system consists of a GS10 scintillator. introduced to UCN instrumentation in [1], coupled to a multi-pixel photon counter (MPPC) [2] to detect the scintillation light. Two versions of this system have been built and installed in different locations around the source as shown in fig. 1. In the one installed in the source's UCN storage vessel (D/E/F), the scintillation light is transmitted through a quartz rod over a total length of 4.12 m to the MPPC. Such a system can directly monitor the UCN before the losses and modifications introduced by the several meter long neutron guides. In the mini-monitor versions (G and J), the scintillator is directly mounted onto the MPPC.

Ultracold neutrons, with energies below 350 neV, undergo reflection from certain materials and can thus be stored in material bottles [3]. This makes them invaluable for precision measurements of fundamental properties of the neutron.

The UCN source at PSI [4–6] started regular operation in 2011. Neutrons are produced via proton-induced spallation on lead with subsequent thermalization in heavy water and conversion to the ultracold regime in 30 liters of solid D_2. After production, the UCN are stored in an intermediate storage vessel, located directly above the solid D_2, from where they can be distributed to experiments via three different, up to 8 m long, UCN guides.

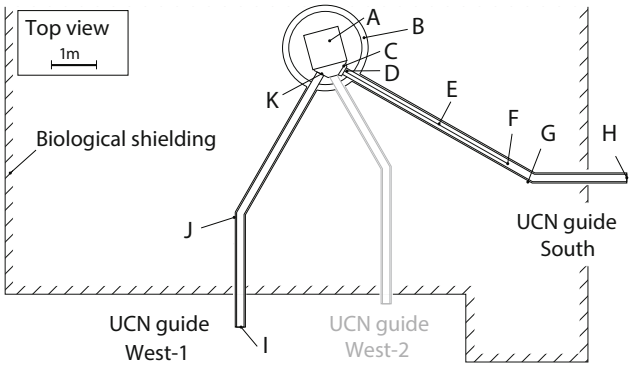

Fig. 1. Layout showing the parts of the PSI UCN source and the locations of the detectors relevant to this work. A: UCN storage vessel; B: vacuum tank; C: vessel valve guide South; D: location of the endoscopic detector; E: light guides for the endoscopic detector; F: location of the MPPCs for the endoscopic detector; G: location of mini-monitor in guide South; H: beam port shutter South; I: beam port shutter West-1; J: location of mini-monitor in guide West-1; K: vessel valve guide West-1.

A several-meter-thick biological shield surrounds the spallation target and the storage vessel and standard UCN detectors can be placed only at the end of the neutron

[a] e-mail: bernhard.lauss@psi.ch

guides, outside this shield. However, it is of great interest to measure the UCN closer to the production area and for this purpose we built a dedicated endoscopic detector for installation in the storage vessel, as well as two mini-monitors placed along the neutron guides. Such a mini-monitor could also be placed inside a UCN experiment vessel.

2 Requirements

Regions around the storage vessel can have radiation levels up to $5 \cdot 10^{11}\,\mathrm{n/cm^2/s}$ due to the spallation process [7] and detector components placed in these regions must be able to withstand this. However, the MPPCs have a low tolerance for radiation [2] thus they must be placed outside this zone, necessitating the use of long light guides.

The high radiation background also requires the detector to be as insensitive as possible to radiation other than the UCN.

The detectors are installed inside the vacuum of the UCN source, hence all components have to be compatible with high vacuum conditions. They also have to be as compact as possible so as to fit in the available space in the source.

Detection of UCN can only be done by conversion, *i.e.* the detected UCN is lost for further experiments. This implies a very small active area of the detector, in order not to induce significant losses.

3 Components of the detector

3.1 GS10 scintillator

The neutrons are detected in a ^{6}Li-doped GS10 glass scintillator, with 18% Li oxide by weight (the Li content is the natural one, 7.5% ^{6}Li, 92,5% ^{7}Li), via absorption as described by the following reaction:

$$\mathrm{n} + {}^6\mathrm{Li} \rightarrow {}^3\mathrm{H} + {}^4\mathrm{He} + 4.78\,\mathrm{MeV}. \quad (1)$$

The α-particle carries away 2.06 MeV and has a range of about 7 μm in the scintillator while the triton with the remaining 2.72 MeV travels up to 40 μm. Part of the energy is transferred to cerium atoms, the scintillating ingredient in the GS10, which have a peak emission wavelength of 395 nm [8]. The scintillation light has a decay time on the order of 100 ns as seen in fig. 2.

The high neutron capture cross-section of some 10^5 barn for UCN in ^{6}Li allows the use of very thin scintillator material while maintaining complete absorption of the UCN. Background signals from gammas or charged particles are reduced in thinner materials, resulting in a better signal-to-noise ratio. For this work, a thickness of 100 μm was chosen as it has been shown [9] to provide good discrimination between UCN and typical backgrounds in experimental areas.

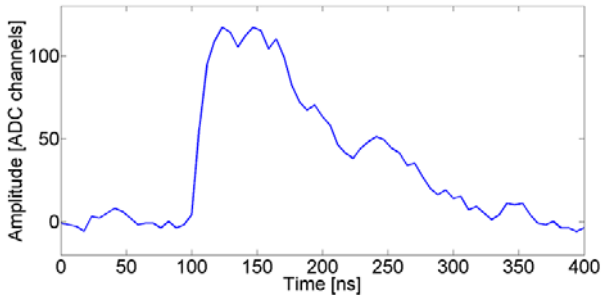

Fig. 2. Typical pulse shape of a neutron capture event in the detector at the output of the amplifier.

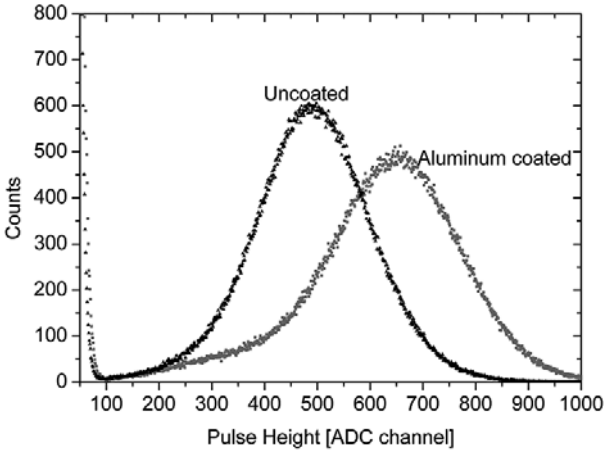

Fig. 3. Pulse-height spectrum (^{252}Cf α source) measured with identical detector setups and exposure times but different scintillators, one coated with Al and one without coating. One can see an increase of the light yield for the coated scintillator. In addition, the energy resolution $\Delta E/E$ (FWHM) of about 0.4 is improved by about 10% by using the coating.

For our purpose, disks with a diameter of 3 mm were laser-cut[1] out of a square sheet of scintillator glass. The disks were then coated with either 200 nm or 500 nm thick layers of aluminum via magnetron sputtering. This layer increases the light collection efficiency by serving as a reflector for the scintillation light. Figure 3 shows the pulse-height spectra (PHS) recorded with a peak-sensing ADC for two scintillator discs, one uncoated and one coated with aluminum. The two spectra were recorded with identical settings of the electronics and the data acquisition system —the advantage of the coating is clearly seen in the increased light yield.

The detector assembly for the storage vessel consists of four scintillators each read out by an MPPC. The scintillators have different coatings: i) 200 nm Al plus 300 nm NiMo, ii) and iii) 500 nm Al, iv) 200 nm Al and 300 nm stainless steel. These coatings were intended to act as energy barriers via their material optical potentials (Al 54 neV, stainless steel 180 neV, and NiMo 230 neV) and thus allow for a crude neutron energy resolution. The GS10 itself has a material optical potential of 84 neV. In the end, the high backgrounds did not allow us to make use of this energy discrimination. The scintillators in the mini-monitors have 200 nm aluminum layer.

[1] `www.mdischott-ap.de`.

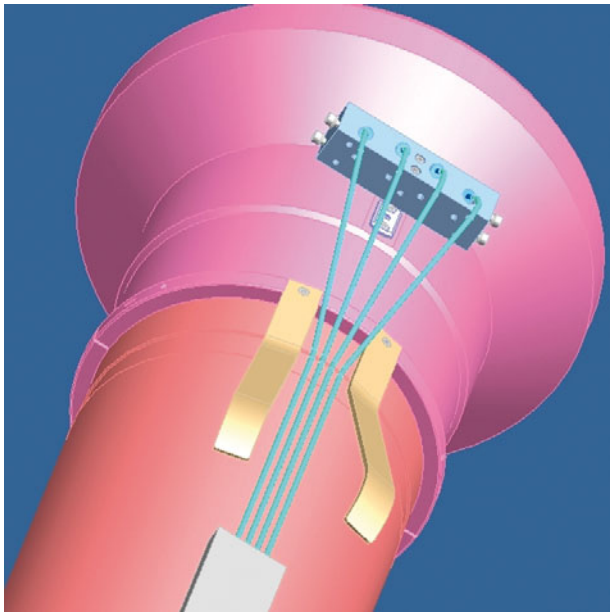

Fig. 4. Drawing of the UCN guide tube close to the storage vessel with attached light-guide system. The ends of the light guides are bent to reach the scintillator mounted and locked in the block made of aluminum (see also fig. 9).

3.2 Light guides

The peak emission wavelength of the GS10 around 395 nm limits the choice of light guide materials. The stringent radiation hardness requirements and the necessary vacuum compatibility further narrows the list of possible materials. The best choice was found to be quartz glass.

The company Heraeus Quarzglas manufactures radiation-hard quartz rods in different grades. The F100 is best suited to our application because of its excellent UV transmission and high resistance to gamma radiation. We tested samples of this glass by irradiating them with thermal neutron fluences up to $10^{15}\,\mathrm{n/cm^2}$ at the PSI neutron irradiation facility (NAA). A close inspection by eye revealed no indication of browning, the latter being the usual sign of radiation damage.

Standard radiation-hard coated quartz fibers would have been much more convenient for handling and installation, however the numerical aperture of such fibers is only 0.22 [10] and unsuitable for our application given the low light yield of the GS10. By using 3 mm solid uncoated quartz rods that match the active area of the MPPCs we gain a factor of ten due to numerical aperture and solid angle.

The quartz rods are available only up to lengths of 1.6 m so several pieces had to be joined together to transport the light over the required distance of about 4 m.

A glassblower[2] fused the quartz rods using an oxyhydrogen flame at a temperature of about 1600 °C. In addition to joining a total of three pieces for each light guide, it was necessary to bend the rods into shape (see fig. 4) in order to adapt them to the geometry of the UCN guide on which they are mounted.

[2] `www.glasform.ch`.

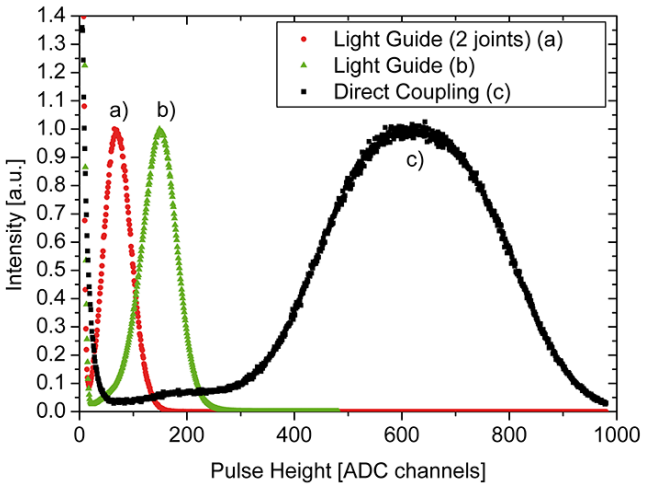

Fig. 5. Comparison of three pulse-height spectra (scaled to equal peak height). Scintillator coupled to the MPPC via a) a light guide with two joints; b) a light guide without joints; c) the scintillator directly coupled to the MPPC.

The scale of light losses induced by the light guides is demonstrated in the ^{241}Am alpha pulse-height spectra (PHS) of three different measurements shown in fig. 5. The largest signal (c)) was obtained by coupling the scintillator directly to the MPPC, the middle peak (b)) was obtained with a 40 cm long light guide, and the smallest signal (a)) was obtained with a light guide of equal length but with two joints, *i.e.* the guide was intentionally broken and rejoined at two positions. One can clearly see the reduction of the light yield. However, it was not possible to characterize the loss very well as measurements showed a large spread: each joint, done by hand, has its individual characteristics and light losses.

3.3 Multi-pixel photon counter

We used Hamamatsu S10362-33-050C multi-pixel photon counters (MPPC), a blue-sensitive device consisting of 3600 avalance photodiodes (APD) each $50\,\mu\mathrm{m} \times 50\,\mu\mathrm{m}$ square, and an overall active area of $3\,\mathrm{mm} \times 3\,\mathrm{mm}$. The semiconductor is encapsulated in a ceramic housing and covered with a thin layer of optical epoxy as shown in fig. 6.

The gain of the MPPC is on the order of 10^6 and it is very sensitive to temperature and supply voltage changes. In our installation inside the UCN source vacuum system the temperature is intrinsically sufficiently stable. Custom-made PSI power supply units provide the required voltage stability. Each pixel of the MPPC generates a signal when it detects a photon and the signal output of the MPPC is the sum of all outputs. MPPCs are capable of measuring very low light quantities down to single photons. The operating principle is thoroughly discussed in [2].

The radiation tolerance of these semi-conductor devices is very low. As shown in [11] a neutron fluence of $10^{11}\,\mathrm{n/cm^2}$ is sufficient to increase the dark count rate

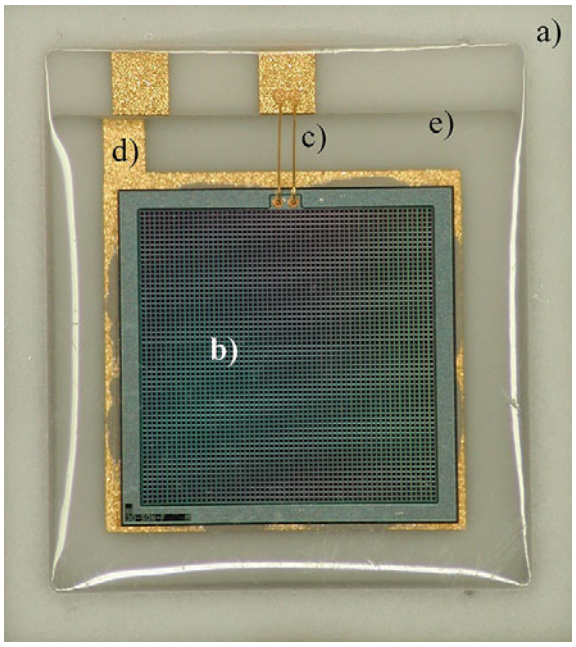

Fig. 6. Close-up of a MPPC: a) ceramic housing; b) pixelated active area; c) bonding wires for the detector voltage; d) grounding pad; e) UV-transparent epoxy glue used to fill the ceramic housing, thus keeping the detector in place.

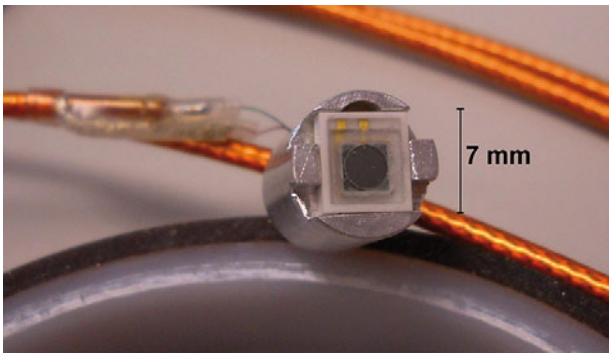

Fig. 7. Mini-monitor: Scintillator glued to an MPPC with the cable attached at the back, ready to be mounted.

and the after-pulse probability. Due to this low radiation hardness the MPPCs have to be placed as far away from the spallation target as possible. The 4 m chosen here was a compromise between reducing the radiation level and limiting the light loss in the light guides.

3.4 Detector construction

The two mini-monitors for the lower radiation zone were made by glueing the scintillators directly to the MPPCs using Epotek 301, an epoxy resin with a very low cut-off wavelength and low outgassing. Figure 7 shows one of the two detectors in an aluminum holder. We have placed these detectors in the 30° bends of the UCN guides South and West-1 where they monitor the UCN flux via 2 mm diameter holes in the bend of the guides (see fig. 1).

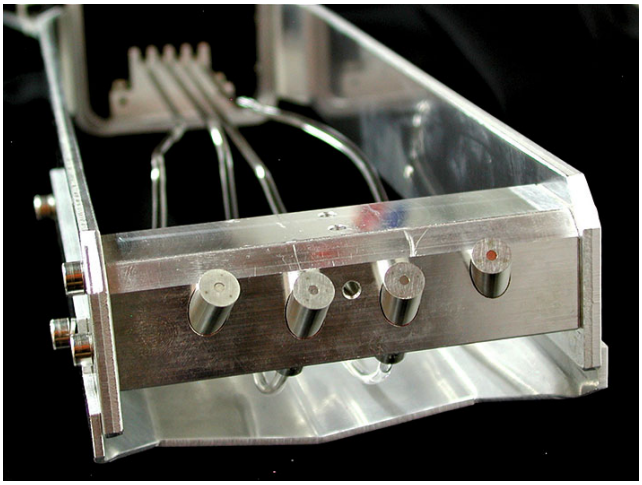

Fig. 8. The front end of the endoscopic detector. The steel cylinders accommodate each the front end of the light guide and a scintillator. A flat steel ring is spot-welded to the top of the capsule to retain the scintillator disc and press it against the guide.

The assembly procedure of the endoscopic detector was more complicated. First, the four light guides were meticulously cleaned using ethyl acetate. Next the gold-plated legs of the MPPCs were clipped and replaced with AWG 32 wire. This wire acts as a mechanical decoupling between the detector and a coaxial cable to which it is connected and which carries the signals to a floating SMA feedthrough. A standard SMA cable delivers the signal to the preamplifiers.

The MPPCs were then glued to the light guides and placed inside a box made of 2 mm thick aluminum plates in order to reduce the amount of electronic pick-up. The box is glued to the detector support —a 4.5 m long aluminum U-profile, which in turn is mounted to the neutron guide— with Torr-Seal, a UHV compatible epoxy resin with good radiation hardness [12].

On the front end of the detector, each scintillator was inserted into a holding capsule followed by the light guide, as shown in fig. 8. This capsule is a stainless-steel cylinder with a smooth 3.05 mm diameter bore. A 0.2 mm thick flat ring with an inner and outer diameter of 2 mm and 3 mm, respectively, was spot-welded to the front end. The ring acts as a catch to press the scintillator against the light-guide end face as seen in fig. 9. Glueing the scintillator to the light guide was out of the question given the intense radiation at this location, and the danger of a fast browning [12] of the glue, with correspondingly large light losses.

The assembled detector was integrated into the front end of UCN guide South (fig. 9) which is part of the UCN storage vessel. There, 2 mm diameter holes allow the detector to view directly inside the storage vessel. The area of four holes corresponds to a surface ratio of 10^{-6}, hence has a negligible influence on the UCN loss. Unfortunately, during the insertion of the guide-detector unit into the source, one of the light guides broke.

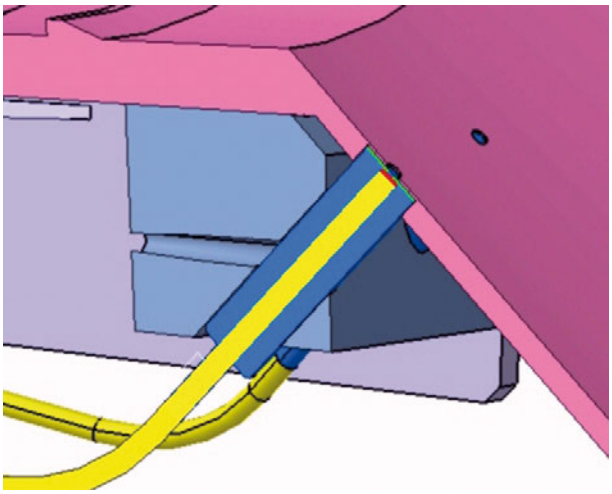

Fig. 9. Design drawing of the detector front end at the end of the UCN guide showing the holder, indicating the stainless-steel capsule with the spot-welded foil (green) containing the scintillator (red) and the light guide (yellow).

4 Electronics

The MPPCs were read out by a custom made PSI preamplifier (reference number GU32_09_1_0). We used a data acquisition system originally designed and produced for the MuCap experiment [13]. The system is based on a flash ADC, which allowed us to record the waveform of every pulse which passed a time-over-threshold (TOT) test, *i.e.* the voltage level exceeded a certain threshold for longer than a given time. The system uses eight Maxim MAX1213 ADCs (170 MHz flash ADC) for eight channels. Four Xilinx Spartan-3 XC3S200-TQ144 field-programmable gate arrays (FPGA), each reading out two flash ADCs, process the data and test for the TOT condition. Pulses which pass the conditions are labeled with a 28 bit time stamp and then sent to one master FPGA which in turn takes care of the communication with the measurement PC via ethernet. The measurements are controlled and recorded within the MIDAS framework[3].

5 Measurements using prototype detectors

5.1 Measurements with α-particles

First tests with the scintillator were done by coupling it directly to a MPPC using index-matching grease. A ^{241}Am α source was used to create scintillation signals. Figure 10 shows the corresponding pulse-height spectrum in the detector.

5.2 Measurements with UCN

A prototype detector consisting of a scintillator coupled to a MPPC via a 1.6 m long quartz rod was tested at the EDM beam line at the PF2 facility [14] of the ILL in Grenoble, France.

The entire setup was placed in a support frame, which in turn was placed inside a Nocasept H5[4] stainless-steel tube. For the test measurements two different pulse-height spectra were recorded. One was the background spectrum, recorded with the shutter towards the UCN turbine closed. In the second measurement, the shutter towards the turbine was open. The resulting pulse height spectra are shown in fig. 11. One can clearly see the difference with UCNs. Furthermore, one can observe an escape peak, which occurs when one of the reaction products of the neutron capture reaction —most likely the triton which has the longer path length— exits the scintillator without depositing most of its energy. This occurs at the end of the track at the Bragg peak.

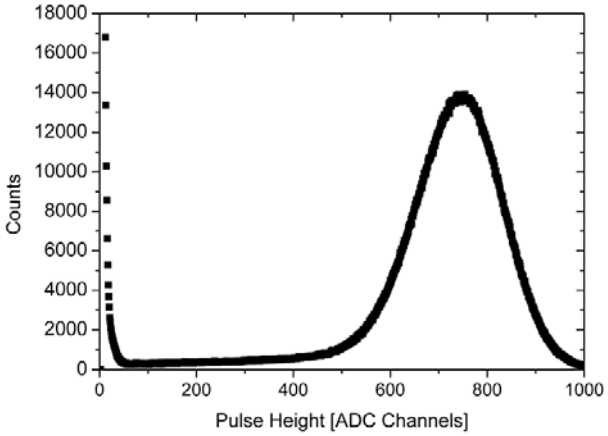

Fig. 10. Pulse-height spectrum of ^{241}Am α-particles impinging on a GS10 scintillator coupled to a MPPC using index-matching grease.

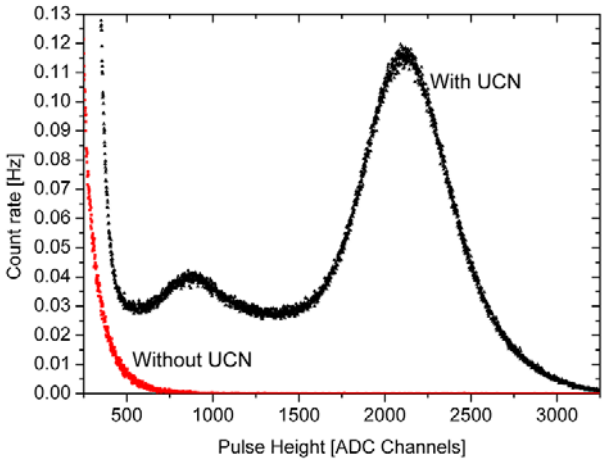

Fig. 11. Pulse-height spectra of the prototype test at ILL (equal exposure time). The upper curve shows the data obtained with UCN. With the shutter closed, no UCN can reach the detector, hence, one can record the background (lower curve).

[3] `midas.psi.ch`.

[4] The material and surface properties of these tubes make them reasonable UCN guides. `www.nocado.com`.

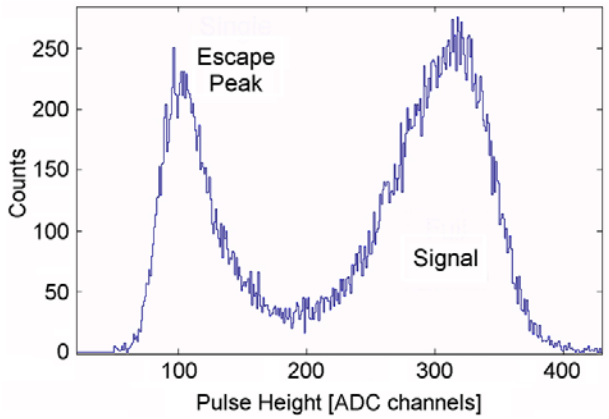

Fig. 12. Pulse-height spectrum of the detector in guide South. The DAQ recorded all pulses which exceeded the time over threshold of 90 ns.

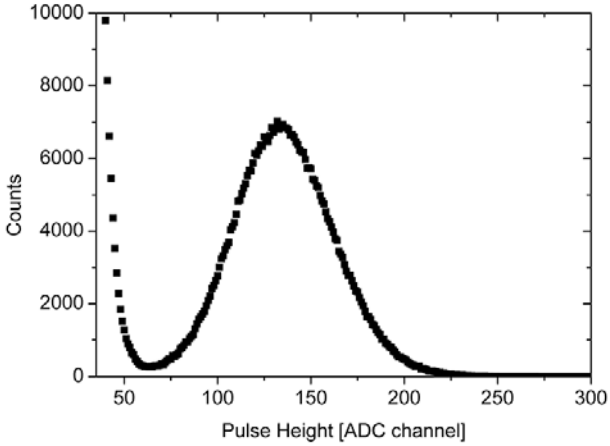

Fig. 13. Pulse-height spectrum of α particles from ^{241}Am deposited inside the capsules to serve as a diagnostic tool. The activity rate is about $0.1\,\mathrm{s}^{-1}$. The scintillator is coated with 500 nm of Al, and coupled to a 4.12 m long light guide. The MPPC is glued to the back end of the light guide.

6 Measurements with the monitor counters

Figure 12 shows the PHS of the mini-monitor placed in guide South. One can clearly see the escape peak and the full-energy peak. The absence of the typical electronic background around zero is due to the cutoff by the FADC data acquisition system. It was set to record only those pulses with a time over threshold of more than 90 ns. The background events typically had a time over threshold of 30–50 ns. This was possible because of the excellent signal-to-noise ratio.

As can be seen from the pulse-height spectrum these detectors show excellent performance. The thresholds can be set clearly above the noise, thus all recorded events can be attributed to neutrons. The time interval over which the proton pulse impinges on the target was excluded from the analysis as there is a very high flux of gammas and fast and thermal neutrons.

A comparision of figs. 11 and 12 shows a much larger escape peak in the PSI measurement and this is currently under investigation. One reason for this could be that at ILL the UCN energy distribution contains more neutrons with higher energies than at PSI. The $1/v$ nature of the neutron absorption cross-section means that UCN with lower velocities are absorbed closer to the scintillator surface. The reaction products then have a higher probability of escaping from the scintillator.

7 Measurements with the endoscopic UCN detector

7.1 Measurements with α-particles

Given the fragility of the endoscopic detector, we wanted to be able to check on its working condition after installation. Therefore, a small amount of ^{241}Am was deposited on the inside of the capsules holding the scintillator leading to a count rate of about $0.1\,\mathrm{s}^{-1}$. This allowed us to check for signals from the α-particles in the detector and determine that three light guides were still functional after the insertion into the source. A PHS of the detector with the best optical transmission properties is shown in fig. 13.

The spectrum differs from the one in fig. 10 in that the plateau between the electronic noise and the peak is much shorter. Due to the large light losses in the guide of almost a factor of 20, the signal approaches the noise. The two other functioning detectors with NiMo and steel coatings showed very low activity from their corresponding α sources and the reason for this is unknown.

7.2 Extraction of the UCN signals in the endoscopic detector

All data taken at the PSI source were recorded with the FADC system described in sect. 4. During proton beam kicks and shortly thereafter, the detector was swamped with signals resembling the neutron signal. The prevalence of the faster neutrons during and after the kick, and the gammas from induced activation, dominate the background making it impossible to separate the UCN events via the usual method of pulse-height discrimination. It should be mentioned that the baseline of the MPPC was very unstable from the beginning of the proton pulse to about 20 s after the pulse. This behavior depended on the proton beam current and the pulse length and became worse with time.

In order to identify the UCN, two measurements were done for each source operation condition, one allowing UCN to enter the storage vessel and one blocking the UCN

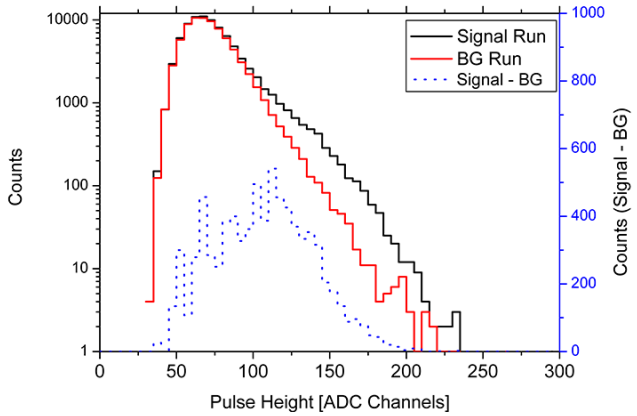

Fig. 14. Pulse-height spectrum with and without UCN in the storage vessel. The dashed line shows the difference spectrum (linear scale on the right) which can be compared with fig. 13.

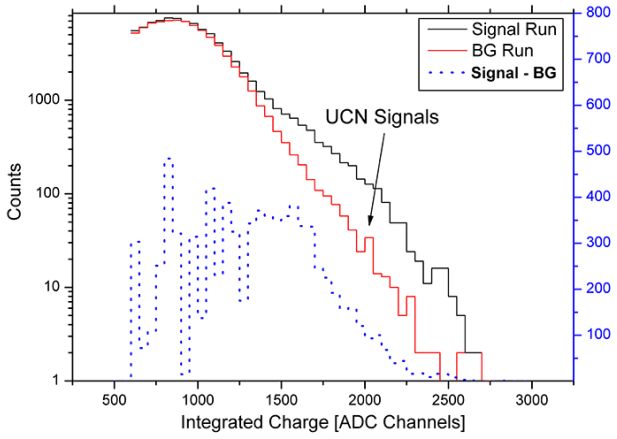

Fig. 15. Charge-integration spectrum with and without UCN in the storage vessel. The dashed line shows the difference spectrum (linear scale on the right).

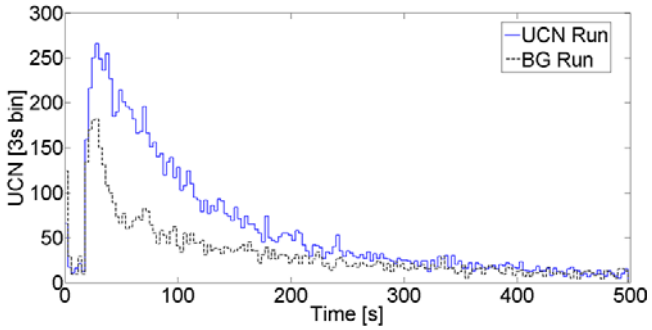

Fig. 16. Comparison of a background run and a UCN run (4 s proton beam pulses). The counts per bin are significantly different for the two measurements. The PHS and charge-integration spectrum in figs. 14 and 15, respectively, are taken from the same measurement runs.

by keeping the shutter at the bottom of the storage vessel closed. Figures 14, 15 and 16 show the results of such a pair of measurements.

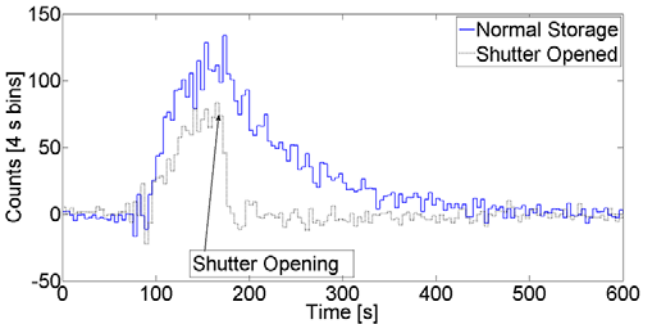

Fig. 17. Two time spectra of the UCN detector. For the dashed line, the UCN shutter at the bottom of the storage vessel was opened after $\sim$ 80 s to show that the count rate originates from UCN. One can clearly see that the rate is reduced with a typical time constant of a few seconds for the open storage vessel shutter.

The waveform data was analyzed with an algorithm which cycled through all the recorded events in several steps. First the baseline was fitted and subtracted. Then a threshold was set on the length and amplitude of the signal candidates. Finally the charge integral for the region spanning 8 channels before the peak, to 20 channels after the signal maximum, was calculated. Once processed, the background data were subtracted from the UCN data. In this way it was possible to extract meaningful data from the aluminum coated scintillator. In the case of the two other detectors with different coatings no event could be clearly attributed to UCN.

In order to demonstrate the correlation of the signals and the presence of UCN in the storage vessel, a measurement was performed in which the UCN shutter at the bottom of the storage vessel was reopened after about 80 s, thus allowing the UCN to fall out of the vessel in a matter of seconds. One can clearly see the associated decrease in the counts in fig. 17.

7.3 Measurement of the storage time constant

One purpose of the detector was to characterize the storage vessel of the source and measure its storage time constant (STC). In order to do this, we filled UCN into the storage vessel keeping all UCN guide valves closed. The large UCN shutter at the bottom of the storage vessel was closed at the end of the filling process and the STC was extracted by observing the decrease of the count rate of the detector. This was done using 4 s long proton pulses for UCN production.

Figure 18 shows the sum of five measurements. After the beam kick the detector signal baseline typically needed 20 to 45 s to stabilize. The fit range was hence chosen from 50 s after the pulse, up to the first channel with fewer than 10 counts per run (fig. 16).

From this we obtain a storage time constant of 85 ± 2 s measured *in situ* in our storage vessel.

Figure 19 shows the count rate of the mini-monitors in guide West-1 and South as a function of time. The UCN

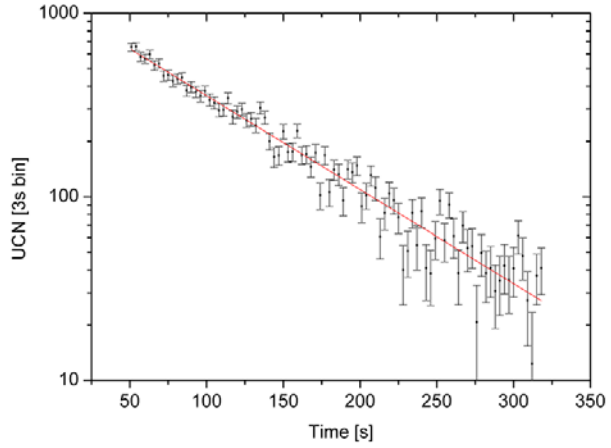

Fig. 18. UCN counts observed in the endoscopic UCN detector after 4 s long proton pulses. Five measurements were added. The single exponential STC fitted to this data is 85 ± 2 s.

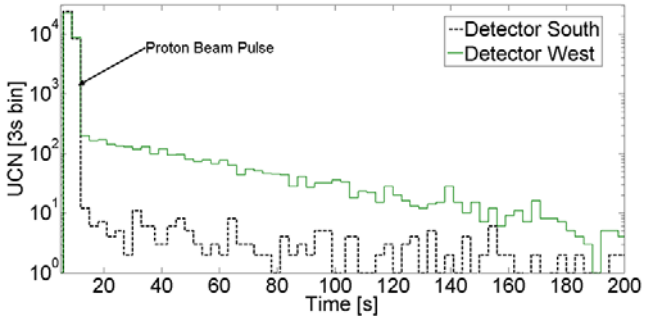

Fig. 19. Counts as a function of time plotted for the detectors in guides West-1 and South. The valve towards guide West-1 was open, the one towards guide South was closed. This corresponds to a STC measurement of the storage vessel combined with guide West-1, STC $= 48 \pm 2$ s.

storage vessel valve of guide West-1 was open and that of guide South was closed; both beam port shutters at the end of the guides were closed. About 3% of the UCN leak through the closed shutter in guide South and gives rise to a signal in detector South.

The detector in guide West-1 monitors the combined volume of the storage vessel and guide West 1. The STC of this space was measured to be 48 ± 2 s. The detector in guide South shows a very faint count rate of a few counts per 3 s bin corresponding to the background and the decreasing UCN counts which leaked through the closed valve.

8 Lifetime of the detector

The condition of a MPPC can be judged by the size of its dark current. A fresh non-irradiated MPPC operated with the nominal voltage of around 70 V will draw about 1–2 μA. Before the diodes were irradiated, the dark current was in this range. Once the beam operation, and thus the irradiation, began the dark current increased gradually. After two months of test operation of the source when only a few proton pulses were generated, the dark current was stable at a level of 15–20 μA. Then, regular beam operation started and at that point the dark current increased to 25–30 μA and the signals ceased to be meaningful. Two month after the annual source shutdown, the dark current was still at a level of 30 μA which is the current limit of the power supply.

9 Conclusion

A detector which can measure the UCN rate and hence the storage time constant of a given UCN vessel has been built. The endoscopic UCN detector is a new device to characterize and monitor UCN count rates in a very high radiation environment.

Despite its handicaps, this first version of an endoscopic UCN detector has proven that it is possible to detect UCN in extreme radiation environments of up to 200 Gray/h and under difficult circumstances. The key to the success of this detector is the employment of long light guides between scintillator and MPPC, the latter have to be placed outside the very high radiation zone. Improving the optical transmission performance of these guides, as well as improving the neutron shielding around the MPPCs, could make such detectors permanent monitoring tools.

The combination of multi-pixel photon counter and glass scintillator is an interesting development in UCN detection. Due to the small size one can use this combination for UCN monitoring tasks or develop a large pixelated UCN detector by combining many MPPCs. This is a magnetically insensitive alternative to PMT-scintillator combinations.

As the PSI UCN source was just starting up when the detector was operated, the UCN count rates were lower than what the detector was initially designed for and the signal-to-noise ratio was unfavorable. Nevertheless, both of our new detector assemblies, the mini-monitor counters and the endoscopic counters could be used to record UCN.

We would like to thank the many people who supported in various ways the presented work: Fritz Burri, Robert Eichler, Peter Geltenbort, Urs Greuter, Michael Horisberger, Thorsten Lauer, Michael Meier, Dieter Renker, Josef Städler, Alexey Stoykov, Alexander Vögele, Jörg Welte, Michael Wohlmuther, the PSI workshops of Urs Bugmann and Max Müller, and Bertrand Blau and the PSI UCN project team. We thank the MuCap Collaboration for lending us the FADC. This work was supported by the Swiss National Science Foundation grant 200020_137664.

References

1. G. Ban *et al.*, J. Res. Natl. Inst. Stand. Technol. **110**, 283 (2005).
2. D. Renker, Nucl. Instrum. Methods A **567**, 48 (2006).
3. R. Golub, D. Richardson, S. Lamoreaux, *Ultra-Cold Neutrons* (Adam Hilger, Publishing Ltd, 1991).

4. A. Anghel *et al.*, Nucl. Instrum. Methods A **611**, 272 (2009).
5. B. Lauss, J. Phys. Conf. Ser. **312**, 052005 (2011).
6. B. Lauss, Hyperfine Interact. **211**, 21 (2012).
7. M. Wohlmuther, S. Teichmann, *Calculation of the dose delivered at the UCN guide west*, Paul Scherrer Institut, Technical Memo TM-85-07-03 (2007).
8. Datasheet: *Lithium glass scintillators (GS10)*, Applied Scintillation Technologies.
9. G. Ban *et al.*, Nucl. Instrum. Methods A **611**, 280 (2009).
10. Datasheet: *Specialty fiber preforms for the most demanding applications*, Heraeus Quarzglas Gmbh & Co KG.
11. I. Nakamura, Nucl. Instrum. Methods A **610**, 110 (2009).
12. J. Bertsch, L. Goeltl, K. Kirch, B. Lauss, R. Zubler, Nucl. Instrum. Methods A **602**, 552 (2009).
13. V.A. Andreev *et al.*, Phys. Rev. Lett. **99**, 032002 (2007).
14. A. Steyerl *et al.*, Phys. Lett. A **116**, 347 (1986).